Arthritis & Rheumatism
DOI 10.1002/art.38295

In vivo imaging of matrix metalloprotease 12 and matrix metalloprotease 13 activities in the mouse model of collagen-induced arthritis.

Ngee Han Lim[1†], Ernst Meinjohanns[2†], George Bou-Gharios[1], Luke L. Gompels[3], Elisa Nuti[4], Armando Rossello[4], Laurent Devel[5], Vincent Dive[5], Morten Meldal[6], Hideaki Nagase[1]

[†]Drs. Lim and Meinjohanns contributed equally to this work.

[1] Ngee Han Lim, PhD, George Bou-Gharios, PhD, Hideaki Nagase, PhD. Kennedy Institute of Rheumatology, Nuffield Department of Orthopaedics, Rheumatology and Musculoskeletal Sciences, University of Oxford, United Kingdom

[2] Ernst Meinjohanns, PhD. Carlsberg Laboratory, Denmark

[3] Luke L. Gompels, MD, PhD. Imperial College London, United Kingdom

[4] Elisa Nuti, PhD, Armando Rossello, PhD. Dipartimento di Farmacia, Università di Pisa, Italy

[5] Laurent Devel, PhD, Vincent Dive, PhD. CEA, Service d'Ingénierie Moléculaire des Protéines (SIMOPRO), Labex LERMIT, 91191 Gif-sur-Yvette, Cedex, France

[6] Morten Meldal, PhD. Nano-Science Center, Department of Chemistry, University of Copenhagen, Denmark

Supported by grants from the Arthritis Research UK, European Union's FP6 CAMP, FP7 LIVIMODE programme, NIH/NIAMS grant AR40994 and Ministero dell'Istruzione dell'Università e della Ricerca, MIUR (Prin 2007).

Corresponding Author: Hideaki Nagase, Kennedy Institute of Rheumatology, University of Oxford, Roosevelt Drive, Headington, Oxford, OX3 7FY UK. E-mail: hideaki.nagase@kennedy.ox.ac.uk Tel: +44 1865612600 Fax: +44 1865612601

Running Title: *In vivo* imaging of MMP-12 and MMP-13 activities in inflammatory arthritis.

Received: Jun 24, 2013; Revised: Sep 30, 2013; Accepted: Nov 21, 2013

Abstract

Objective. To develop enzyme activatable Förster resonance energy transfer (FRET) substrate probes to detect MMP-12 and MMP-13 activities *in vivo* in mouse models of inflammatory arthritis

Methods. Peptidic FRET probes activated by MMP-12 and MMP-13 were reverse designed from inhibitors selected from a peptide phosphinic inhibitor library. Selectivity of the probes was demonstrated *in vitro* using MMP-1, MMP-2, MMP-3, MMP-12, and MMP-13. *In vivo* activation of the probe was tested in the zymosan-induced mouse model of inflammation and probe specificity was evaluated by the metalloprotease inhibitor GM6001 and specific synthetic inhibitors of MMP-12 and MMP-13. The probes were used to follow these enzyme activities in the collagen-induced arthritis (CIA) model *in vivo*.

Results. The MMP-12- and MMP-13-activity probes (*MMP12ap* and *MMP13ap*, respectively) discriminated between the two enzymatic activities. The *in vivo* activation of these probes was inhibited by GM6001 and by their respective specific inhibitors. In the CIA model, *MMP12ap* activation peaked 5 days after disease onset and showed strong correlation with disease severity during this time ($r = 0.85$; $p < 0.0001$). *MMP13ap* activation increased gradually after disease onset and correlated with disease severity over a longer period of 15 days ($r = 0.58$; $p < 0.0001$).

Conclusion. We have generated two selective FRET probes that can be used to follow MMP-12 and MMP-13 activities in live animals. *MMP12ap* follows the initial stage of inflammation in CIA, while *MMP13ap* follows the progression of the disease. The specificity of these probes is useful in monitoring the efficacy of MMP inhibitors.

Rheumatoid arthritis (RA) is a chronic systemic autoimmune disease that mainly affects joints. It is characterised by synovial inflammation, with infiltration of immune cells and hyperplasia of synovial cells, followed by destruction of articular cartilage and joint dysfunction. The matrix metalloproteases (MMPs), a family of zinc dependent metalloendopeptidases many of which are capable of degrading components of the extracellular matrix (1), are involved in multiple stages of the progression of RA (2). Detection of the different MMP activities *in vivo* may offer novel ways of following the pathogenesis of RA in the clinic.

Early in the pathogenesis of RA, there is an increase in the number of macrophages infiltrating the synovium and the extent of infiltration correlates with disease severity (3). A unique MMP associated with macrophages is MMP-12, or macrophage metalloelastase (4). Concurrent with the increase of macrophages in the synovium, there is an increased expression of active MMP-12 associated with these macrophages in RA patients (5). Transgenic rabbits overexpressing MMP-12 showed increased synovial hyperplasia, pannus formation, and articular cartilage degeneration in inflammatory arthritis (6). Detection of MMP-12 activity could be a surrogate marker for macrophage infiltration in RA. Articular cartilage destruction, on the other hand, occurs later in the pathogenesis of RA, and several MMPs are involved in the degradation of type II collagen in articular cartilage (2). In mice, the major collagen-degrading enzyme is MMP-13, or collagenase 3. Inhibition of MMP-13 decreased erosion in models of RA (7) and mice lacking MMP-13 are protected from cartilage damage in an osteoarthritis model (8). Detection of MMP-13 activity would be a marker for tissue destruction in RA, at least in murine models of arthritis.

The activities of these MMPs in disease pathology have so far been inferred from limited snapshots which are affected by several aspects that govern activity, including transcription, post translational modification, endocytosis, activation of the MMP and their

inhibition by endogenous inhibitors (9-11). *In vivo* optical imaging allows the sum of these processes on the activities of the MMPs to be measured in real time through the use of near-infrared fluorophores (NIRFs), as fluorescence is detected in the NIR-window of the spectrum where tissue is largely transparent and may be detected up to a depth of about 1 cm (12). This makes NIRF-optical imaging suitable for small animal imaging and in the joints of the hands and feet in the clinic. We chose to develop probes specific for MMP-12 and MMP-13 to follow the activities of these enzymes during the progression of RA, as they represent macrophage migration and cartilage collagen degradation.

There are several designs of probes for detecting protease activity *in vivo* (13). Activity-based probes are chemical compounds that act as an irreversible inhibitor of the protease by covalently modifying their targets with the fluorophore. Some of these have been developed for cysteine proteases (14-16). However, detection of low abundance proteases by this approach is limited, as these probes do not multiply signals through catalysis. Substrate-based probes, on the other hand, overcome this limitation by amplifying the signal from a single enzyme. These consist of peptides which have a NIRF attached to one side of the proteolytic cleavage site and a FRET quencher on the other. These have been developed for cysteine (17-19), serine (20) and metallo- (21) proteases. A drawback of using substrate-based probes is that the products do not necessarily stay in the vicinity of the enzyme. To overcome this limitation, peptide substrates flanked on one side by a cationic cell penetrating peptide with a NIRF and on the other by an anionic sequence with a quencher have been developed (22). Upon proteolysis, the cleaved cationic fragment with the NIRF interacts with the lipid membrane and penetrates into the cell. Another method of limiting product diffusion is to incorporate multiple substrates on large polymeric scaffolds, which have been developed to detect a broad range of MMPs (21) and cathepsins (17). Recent developments for

substrate-based probes include the reverse design of specific tight-binding inhibitors into peptide substrates of cysteine cathepsins (23).

To develop selective MMP-12 and MMP-13 probes, we screened a phosphinic peptide inhibitor library for high affinity inhibitors and reverse designed the inhibitors into selective FRET peptide substrates for these metalloproteases. The specificity of these substrates for MMP-12 and MMP-13 were confirmed *in vitro* and *in vivo.* These substrates, *MMP12ap* and *MMP13ap*, were then used to characterise MMP-12 and MMP-13 activities in the collagen-induced arthritis (CIA) model of RA. The combination of the two probes demonstrates the longitudinal changes in the activity of these two distinct MMPs during progression of the disease.

Materials and methods

Synthesis and screening of inhibitor libraries

The synthesis of the phosphinic peptide inhibitor library and its screening method were described previously (24). In essenseessence, the solid phase combinatorial library of ~500,000 phosphinic peptides was constructed on polyethlyepolyethylene glycol polyacrylamide (PEGA) resin using a one-bead-two-compounds approach, where each bead contained a general FRET MMP substrate and a putative phosphonic peptide inhibitor. Upon incubation with MMP-12 or MMP-13, beads containing a weak inhibitor fluoresce, whereas beads containing a strong inhibitor remain dark. The inhibitor sequence on the dark beads was determined by MALDI-TOF mass spectrometry and the identified sequence used to generate peptide substrates for MMP-12 and MMP-13.

MMP-12 and MMP-13 FRET peptide substrate synthesis

Peptides were synthesized by multiple-column peptide synthesis on $PEGA_{800}$ resin in a 20 column synthesis block (25). Briefly, Fmoc-Gly-OH was coupled to $PEGA_{800}$ resin (0.2 mM/g) in an *o*-(benzotriazol-1-yl)-*N,N,N′,N′*-tetramethyluronium tetrafluoroborate (TBTU) (2.8 equivalents) and N-ethylmaleimide (NEM) (4 equivalents) coupling step. Fmoc was removed by treatment with 20% piperidine in dimethylformamide (DMF). The FRET substrates were synthesized by coupling after preactivation of N^{α}-Fmoc amino acids (3 equivalents) with TBTU (3 equivalents) and NEM (4 equivalents) using the following side chain protecting groups for the N^{α}-Fmoc-amino acids: *O*-*t*Bu for Asp and Glu; *t*Bu for Tyr, Ser and Thr; Trt for Cys, Asn and Gln; Boc for His, Lys and Trp; and Pmc for Arg. Each coupling step was carried out for 3 h using 3 equivalents of the preactivated amino acid in 0.5 volumes of DMF. In difficult couplings, 0.2 equivalents of 3,4-dihydro-3-hydroxy-4-oxo-1,2,3-benzotriazine was added as an acylation catalyst and indicator of reaction completeness. Reaction completion was further assessed using the Kaiser test. Two equivalents of the preactivated amino acid were added to coupling reactions that were incomplete. The terminal amino protecting Fmoc was removed by piperidine treatment. Peptides were cleaved from the resin and side-chain deprotection groups were removed by treatment with trifluoroacetic acid (TFA): thioanisole: ethanedithiol: water (87.5:5:2.5:5). FRET substrates were purified by reverse phase HPLC with a DeltaPak C18 column and a linear gradient of 0-90% acetonitrile with water containing 0.1% TFA on a Waters HPLC system (Hertfordshire, UK).

In vivo probe assembly

The *in vivo* probes were synthesized using the synthesis protocol described in the previous section with the following modifications to incorporate the Cy 5.5 fluorophore and QSY21 quencher. The base labile linker hydroxymethylbenzoic acid was coupled to the $PEGA_{800}$ resin (0.4 mM/g) by TBTU (2.9 equivalents) and NEM (4 equivalents) with a

preactivation for 1 min and coupling for 2 h. The Fmoc-Gly-OH amino acid (3 equivalents) was coupled by 1-(mesitylene-2-sulfonyl)-3-nitro-1,2,4-triazole (3 equivalents) and methylimidazole (6 equivalents) with a preactivation for 1 min and esterification for 2 h. The first lysine was protected with the (4-methoxyphenyl)-diphenylmethyl (MMT) group. The terminal Fmoc group was removed with 20% piperidine in DMF and the protected peptide cleaved from the resin by 0.1% NaOH. The QSY21 quencher was coupled for 12 hours to the terminal amino group by using QSY21-NHS ester (1.2 equivalents) in DMF and addition of *N,N*-diisopropylethylamine (DIPEA). The QSY-21 labeled peptides were purified by semi-preparative HPLC under neutral conditions before being subjected to moist 0.5% TFA in CH_2Cl_2 for 15 min to remove MMT. The Cy5.5 fluorophore was coupled to the side chain amino group of lysine by succinimide ester coupling using Cy5.5-OSu in DMF with DIPEA for 12 hours. The NIRF-labeled peptides were deprotected with 95% TFA in water for 2 hours.

Characterization of peptides

Peptides were purified by HPLC and analyzed by ESI-MS on a QTOF Waters Global Ultima (Hertfordshire, UK), using aqueous acetonitrile with 0.2% formic acid for the eluting spray. Individual products analyzed were as follows. *MMP12-1*, Y(NO_2)GPLG~LEEAK(Abz)G-NH_2 ($C_{58}H_{86}N_{15}O_{19}$): 0.168 Rf; MS(ESI) 1296.6224$[M+H]^+$ calculated, found 1296.5868. *MMP12-2*, Y(NO_2)YIYG~LTMPGK(Abz)G-NH_2 ($C_{72}H_{101}N_{16}O_{19}S$): 0.198 Rf; MS(ESI) 1525.7150$[M+H]^+$ calculated, found 1525.7172. *MMP13-1*, Y(NO_2)GPLG~MRGLK(Abz)G-NH_2 ($C_{58}H_{89}N_{17}O_{16}S$): 0.177 Rf; MS(ESI) 1311.6394$[M+H]^+$ calculated, found 1311.6251. *MMP13-2*, Y(NO_2)GPAG~LYEK(Abz)G-NH_2 ($C_{56}H_{75}N_{13}O_{18}$): 0.154 Rf; MS(ESI) 1216.5353$[M+H]^+$ calculated, found 1216.5903.

For MS analysis of the NIRF substrates, sodiated species of the sulfate groups in Cy5.5 were observed in various amounts. Due to two internal positive charges, species were observed as double- and triple-charged under acidic conditions. The most prevalent ions were as follows. *MMP12ap*, QSY-21-GPLG~LEEAK(Cy5.5)G-OH ($C_{124}H_{141}N_{16}Na_3O_{32}S_5$): 0.104 Rf; MS(ESI) 1298.8342$[M]^{++}$/2 calculated, found 1298.8356 and 873.8271$[M+H]^{+++}$/3. *MMP13ap*, QSY-21-GGPAG~LYEK(Cy5.5)G-OH ($C_{124}H_{138}N_{16}Na_4O_{31}S_5$): 0.124 Rf; MS(ESI) 1299.3949$[M]^{++}$/2 calculated, found 1299.3801 (also: 1288.3898(3 Na^+) and 1277.4134(2 Na^+)).

Enzyme assays

Catalytic domains of MMP-1 (MMP-1_{cat}), MMP-3 (MMP-3_{cat}), full-length MMP-2, full-length MMP-12 and full-length MMP-13 were prepared as previously described (26-28). The MMP-12 specific inhibitor (MMP-12i), RXP470 is the phosphinic peptide inhibitor described as compound 1 in Devel *et al.* (27), and the MMP-13 specific inhibitor (MMP-13i), EN211 is the N-O-isopropyl sulfonamido based hydroxamate described as compound 5 in Nuti *et al.* (29).

The rates of cleavage of the peptides by different MMPs were determined by incubation of 1 μM of the peptides (*MMP12-1, MMP12-2, MMP13-1, MMP13-2*) with 1 nM of the enzymes (MMP-1_{cat}, MMP-2, MMP-3_{cat}, MMP-12 or MMP-13) in 50 mM Tris-HCl pH 7.5, 150 mM NaCl, 10 mM $CaCl_2$, 0.02% NaN_3, 0.05% Brij-35 at 37 ^oC for 1 hour. Steady-state cleavage of the substrates was continuously monitored by reading the emission at 393 nm following excitation at 325 nm using a fluorescence plate reader (Spectramax, Molecular Devices, California, USA). The fluorescence of completely cleaved substrate was used to convert fluorescence units into mols. The K_M values of the substrates for MMP-12

and MMP-13 were determined by incubation of 1 nM of enzyme with a range of substrate concentrations (250 nM-64 μM) for 30 mins. The rates of substrate hydrolysis were calculated and the data fit to the following equation to obtain the K_M and maximal velocity (V_{max}) using the software Prism (version 5.0, Graphpad Software, La Jolla, USA): $v= (V_{max} x[S])/(K_M+[S])$. The k_{cat} value was derived from $k_{cat}= V_{max}/[E]$.

Animal models

Male C57BL/6J mice and DBA/1 mice aged 10 weeks were purchased from Harlan Laboratories (Blackthorn, Bicester, UK). Mice were housed in groups of 6 in individually vented cages, maintained at 21 ± 2 ^{o}C on a 12-hour light/dark cycle with food and water provided *ad libitum*. All experimental protocols were performed in compliance with the UK Animals (Scientific Procedures) Act 1986 regulations for the handling and use of laboratory animals (PPL: 70/6533).

Paw oedema was induced by injection of 20 μg of Zymosan A in sterile PBS (Sigma-Aldrich, Dorset, UK) into the right hind foot pad of 10 week old male C57BL/6J mice following induction of anaesthesia by gaseous anaesthetic (2% isofluorane and O_2). Two days post injection, probes were delivered either intraplantar (10 μl of 1 μM of probe with or without inhibitors [10 μM GM6001, 1 μM MMP-12i or 1 μM MMP-13i]) or intravenously via the tail vein (150 μl of 1 μM probe). The amount of probe injected was based on the compromise between detection, possible toxicity and cost; a test injection of 5-times more probe intravenously yielded a corresponding 5-fold increase in signal with no observable side-effects (data not shown). Two, 4, 8 and 16 hours after injection, fluorescence images of the mice were obtained by capturing the emission at 700 nm for 1 min after exposure at 630

nm under gaseous anaesthesia (2.5% isofluorane and O_2) in a Kodak *In Vivo* FX Pro (Carestream, Woodbridge, USA).

For the CIA model, 10-week old DBA/1 mice were immunized by injections intradermally at the base of the tail with an emulsion of 200 μg bovine type II collagen in 100 μl of Freund's complete adjuvant. Arthritis was assessed daily by scoring each limb of the mice according to Inglis *et al.* (30) with the following criteria: 0 –normal; 1 –slight swelling and erythema; 2 –pronounced edematous swelling and 3 –joint rigidity. The thickness of each hind paw was also measured with microcalipers (Kroeplin, Schluchlem, Germany). Three, 5, 10 or 15 days after the onset of arthritis, 150 μl of 1 μM probe was delivered intravenously via the tail vein. Four hours after injection, fluorescence images of the mice were obtained.

Image and statistical analysis

Fluorescence images were analysed using the Carestream MI software (version 5.1). Regions of interest (ROI) were defined using the wand tool to encompass the entire hind paw. The mean fluorescence intensity (MFI) of the ROI was obtained. Fluorescence images shown are false coloured using the rainbow spectrum, with the range indicated in the figures. All statistical analysis was carried out using Prism Software using paired student's t-tests, one way ANOVA with Bonferroni post-tests and Pearson correlation where indicated.

Results

Selection of FRET substrates by reverse design of inhibitors

Screening the phosphinic peptide inhibitor bead library with MMP-12 yielded the sequences GPLG[PO_2H-CH_2]LEEA and YIYG[PO_2H-CH_2]LTMPG as MMP-12 inhibitors. These were reverse designed and synthesised as the *MMP12-1* (Y(NO_2)GPLGLEEAK(Abz)G) and *MMP12-2* (Y(NO_2)YIYGLTMPGK(Abz)G) FRET

substrates. Screening the same library with MMP-13 yielded the sequences GPLG[PO_2H-CH_2]MRGL and GGPAG[PO_2H-CH_2]LYEK. Similar reverse design lead to the *MMP13-1* (Y(NO_2)GPLGMRGLK(Abz)G) and *MMP13-2* (Y(NO_2)GGPAGLYEK(Abz)G) FRET substrates respectively.

In vitro activation of probes

We tested the activation of the four peptide substrates *MMP12-1, MMP12-2, MMP-13-1* and *MMP13-2 in vitro* by various MMPs. The results are summarised in Table 1. The *MMP12-1* substrate was cleaved 10-times more rapidly by MMP-12 than by MMP-13 and between 40-75-times more rapidly by MMP-12 than by MMP-1, MMP-2 or MMP-3. *MMP12-2* was cleaved by MMP-12 30 times more rapidly compared to all the other MMPs tested. *MMP13-1* was poorly cleaved by all the MMPs tested, whereas *MMP13-2* was cleaved 2-times more rapidly by MMP-13 than by MMP-12, and between 10-20-times more rapidly by MMP-13 than by MMP-1, MMP-2 or MMP-3.

The kinetic parameters for the cleavage of the FRET substrates by MMP-12 and MMP-13 were determined. *MMP12-1* was cleaved by MMP-12 with a K_M of 91.51 μM and a k_{cat} of 4.51 s^{-1}. *MMP12-2* was cleaved by MMP-12 with a K_M of 110.5 μM and a k_{cat} of 3.35 s^{-1}. No concentration dependent cleavage of *MMP13-1* was detected, indicating that the inhibitor peptide was unsuitable as a substrate, whereas *MMP13-2* was cleaved by MMP-13 with a K_M of 58.4 μM and k_{cat} of 4.34 s^{-1}. The substrates *MMP12-1* and *MMP13-2* were selected for conversion into *in vivo* probes and the fluorophore and quencher pair were switched to Cy 5.5 and QSY-21. These *in vivo* substrates will henceforth be referred to as *MMP12ap* for the MMP-12 activity probe and *MMP13ap* for the MMP-13 activity probe. The chemical structures of these are shown in Figure 1A. Retention of the specificity of cleavage of these *in vivo* probes was qualitatively shown by incubation of 1 μM of the

substrate with 50 nM of the respective MMPs for 30 min and the reaction spotted on a glass slide and imaged, shown in Figure 1B.

In vivo activation of probes in acute inflammation.

The zymosan-induced paw oedema model of acute inflammation was used to test probe activation *in vivo.* After intraplantar injection of 150 µl of 1 µM probes two days after the zymosan injection, both *MMP12ap* and *MMP13ap* were found to be activated in a time-dependent manner (representative images from a single mouse shown in Figure 2A). Quantification of the MFI of the whole paw showed that the signal from *MMP12ap* peaked 8 hours after probe injection at 11600 units, whereas the signal from *MMP13ap* peaked 4 hours after injection at 6700 units (Figure 2B). Co-injection with the broad-spectrum MMP-inhibitor GM6001 at 10-times the probe concentration inhibited the cleavage of these probes, indicating that MMPs were largely responsible for the observed increase in fluorescence.

Further validation of the specificity of probe activation *in vivo* was achieved by co-injection of the specific inhibitors MMP-12i and MMP-13i. Co-injection of 1 µM MMP-12i with 1 µM *MMP12ap* showed that it competed with the probe at the early time periods (0-2 hours) and achieved full inhibition of probe activation by 8 hours (Figure 2B) whereas co-injection of 1 µM MMP-13i did not have a significant effect on activation of *MMP12ap*. Activation of *MMP13ap* was effectively inhibited by co-injection with 1 µM MMP-13i or 10 µM GM6001 for 2 hours after injection (Figure 2B). However, this inhibition of probe activation was not maintained at later time points. This loss of inhibition could be due to enzyme turnover or clearance of inhibitor. MMP-12i had no effect on the activation of *MMP13ap*. These data indicate that MMP-12 and MMP-13 are mostly responsible for *MMP12ap* and *MMP13ap* activation respectively in the inflamed paws.

To apply the *MMP12ap* and *MMP13ap* probes to other systemic disease models such as the CIA, intravenous delivery of the probes was first tested in the zymosan model of rapid inflammation. Upon intravenous injection of 150 µl of 1 µM of either probe, there was a transient increase in fluorescent intensity over time in the inflamed paw for both probes, with maximum differentiation of the inflamed paw compared to the contralateral paw at 4 hours (Figure 2C). A maximum MFI of 6000 units for *MMP12ap* and 13300 units for *MMP13ap* was observed at 4 hours in the inflamed paw (Figure 2D). Increased fluorescence was detected in the contralateral paw, presumably due to circulation of activated probe (increased from a background of 500 units to between 3000-4000 units for *MMP12ap* and 5000-8000 units for *MMP13ap*). However, the signal continued to be significantly higher in the inflamed paw 4 and 16 hours after injection of *MMP12ap*, and 4, 8 and 16 hours after injection of *MMP13ap*. This signal was 1.5 and 1.9-times higher at 4 hours in the inflamed paw than in the contralateral paw for *MMP12ap* and *MMP13ap*, respectively. These data indicate that probes delivered via the tail vein are activated mainly in inflamed paws.

In vivo activation of probes in the CIA model.

In the CIA model, 68% of animals had at least 1 swollen paw 45 days after induction (49/72, Figure 3A). In the animals that developed disease, the summed scores of disease severity 3, 5, 10 and 15 days after onset of inflammation are shown in Figure 3B, left y-axis. Disease severity as described by the thickness of the hind paws followed that of the summed clinical scores (Figure 3B, right y-axis). Typical images obtained using the *MMP12ap* and *MMP13ap* together with their individual clinical scores are shown in Figure 3 C and 3 D, respectively. Both the incidence of disease and the amount of signal obtained from the fore paws were lower than from the hind paws. We therefore excluded the data from the fore paws in this study.

The amount of *MMP12ap* activation in each inflamed hind paw 3, 5, 10 and 15 days after onset of inflammation is shown in Figure 4A. The amount of probe activation correlated with the amount of swelling observed when the probe was delivered 3 and 5 days after onset of disease, with the Pearson correlation coefficient, *r,* of 0.991 at 3 days ($p = 0.009$) and 0.759 at 5 days ($p = 0.006$). There was no significant correlation 10 and 15 days after onset of disease, with an *r* of -0.031 ($p= 0.953$) and 0.488 ($p = 0.512$) respectively. The correlation was strongest when the data from 3 days and 5 days after onset is taken together, with an *r* of 0.847 ($p <0.0001$), but became weaker when all time points were taken together ($r = 0.416$, $p = 0.039$). The correlation data is summarised in Table 2. This indicates that *MMP12ap* was most useful at classifying disease severity at an early window of up to 5 days after onset of disease. Activation was also highest at 5 days after onset, with a MFI of 1630 units (Figure 4C).

MMP13ap activation in individual inflamed hind paws 3, 5, 10 and 15 days after onset of inflammation is shown in Figure 4B. The correlation between *MMP13ap* activation and paw swelling is summarised in Table 2. Looking at the individual days, correlation between probe activation and paw swelling was only significant on day 5, which had an *r* of 0.833 ($p = 0.02$). However, when all the data were taken together, the correlation between *MMP13ap* activation and disease severity was significant at an *r* of 0.561 ($p <0.0001$). This indicated that *MMP13ap* was better at classifying disease over a wider timeframe than *MMP12ap*. Activation of *MMP13ap* was highest 15 days after onset, with a MFI of 1300 units (Figure 4D).

The versatility, specificity and signal intensity of the *in vivo* probes presented here will allow the monitoring of joint damage throughout the development of arthritis. *MMP12ap* can be used to follow the initial stages of inflammation; whereas the *MMP13ap* can be used throughout disease progression.

Discussion

We have characterised two peptide sequences that are selectively cleaved by MMP-12 and MMP-13, respectively, through the reverse design of MMP-12- and MMP-13-specific phosphinic inhibitors. These sequences were synthesised as the NIRF-FRET *MMP12ap* and *MMP13ap* substrate probes. Using these probes in live animals, we have demonstrated that there is clear temporal regulation of MMP-12 and MMP-13 activity in the CIA model of arthritis, with an early peak in MMP-12 activity, followed by later MMP-13 activity. Additionally, activation of *MMP12ap* correlated strongly with early disease progression and activation of *MMP13ap* correlated over a wider period of disease progression.

Previously, immunohistochemistry has shown that there is an increased expression of MMP-12 associated with the inflammatory macrophages lining the synovium of RA patients (5). With *MMP12ap*, we have visualised an increase in MMP-12 activity in live animal joints. This activity peaks 5 days after onset of CIA and declines by 10 days. This is similar to that observed through immunohistochemistry in the rabbit model of RA (6). MMP-12 may also activate other MMPs, such as MMP-2 and MMP-3 (31). Indeed, MMP-3 activity, as detected by a polymeric MMP-3-substrate probe, peaked 5 weeks after immunisation in an inflammatory model of arthritis (32), suggesting that MMP-3 activation follows from macrophage-derived MMP-12 activity. The eventual down-regulation of MMP-12 activity after macrophage infiltration may serve to limit pro-inflammatory cytokines processing by MMP-12 (33). *MMP12ap* is therefore an early marker for the infiltration of activated macrophages into tissue. Detection of macrophage infiltration using positron emission tomography has been suggested as a means to diagnose arthritis before clinical symptoms manifest (34). *MMP12ap*, on the other hand, serves as a cheaper, less damaging method to detect early macrophage infiltration.

MMP-13 is a terminal effector of cartilage degradation due to its ability to degrade the type II collagen component of cartilage (11). The breakdown product of type II collagen can be monitored in the serum of RA patients and have been shown to correlate with the amount of radiological damage (35). Overexpression of MMP-13 in mice results in degradation of articular cartilage (36). Gene expression profiling of paws of mice with CIA also indicated that MMP-13 was up-regulated at the peak to declining stage of the disease (37). With *MMP13ap*, we have managed to visualise this later activity *in vivo* in CIA and shown that it correlates quantitatively with disease progression. Another peptide-substrate probe detecting MMP-13 activity was used in a rat model of osteoarthritis (38) and correlated qualitatively with the progression of cartilage degradation. These studies emphasises the potential of *MMP13ap* as a marker for quantifying cartilage degradation during arthritis.

Different MMPs are involved in various stages of both biological and pathophysiological processes (39). With *MMP12ap* and *MMP13ap*, we have shown that it is possible to delineate these different activities *in vivo*. Protease-specific activatable probes that are detectable *in vivo* are important tools to monitor disease progression and the efficacy of protease-inhibitor therapeutics as they allow multiple measurements of net protease activity. Inhibitors of MMPs need to be highly selective and potent at low doses, as off-target effects and lowering of dosages have produced negative results in clinical trials (40). MMP-specific activatable probes may be used during the testing of inhibitors, both to determine effective dosages and to study off-target effects. Within the limitations of fluorescent imaging technology, well-characterised and validated protease-specific activatable probes offer the potential to tailor treatment to particular phases of arthritic disease.

References

1. Nagase H, Visse R, Murphy G. Structure and function of matrix metalloproteinases and TIMPs. Cardiovasc Res. 2006;69(3):562-73.
2. Murphy G, Nagase H. Reappraising metalloproteinases in rheumatoid arthritis and osteoarthritis: destruction or repair? Nat Clin Pract Rheum. 2008;4(3):128-35.
3. Yanni G, Whelan A, Feighery C, Bresnihan B. Synovial tissue macrophages and joint erosion in rheumatoid arthritis. Ann Rheum Dis. 1994;53(1):39-44.
4. Shapiro SD, Kobayashi DK, Ley TJ. Cloning and characterization of a unique elastolytic metalloproteinase produced by human alveolar macrophages. J Biol Chem. 1993;268(32):23824-9.
5. Liu M, Sun H, Wang X, Koike T, Mishima H, Ikeda K, et al. Association of increased expression of macrophage elastase (matrix metalloproteinase 12) with rheumatoid arthritis. Arthritis Rheum. 2004;50(10):3112-7.
6. Wang X, Liang J, Koike T, Sun H, Ichikawa T, Kitajima S, et al. Overexpression of human matrix metalloproteinase-12 enhances the development of inflammatory arthritis in transgenic rabbits. Am J Pathol. 2004;165(4):1375-83.
7. Jungel A, Ospelt C, Lesch M, Thiel M, Sunyer T, Schorr O, et al. Effect of the oral application of a highly selective MMP-13 inhibitor in three different animal models of rheumatoid arthritis. Ann Rheum Dis. 2010;69(5):898-902.
8. Little CB, Barai A, Burkhardt D, Smith SM, Fosang AJ, Werb Z, et al. Matrix metalloproteinase 13-deficient mice are resistant to osteoarthritic cartilage erosion but not chondrocyte hypertrophy or osteophyte development. Arthritis Rheum. 2009;60(12):3723-33.
9. Hadler-Olsen E, Fadnes B, Sylte I, Uhlin-Hansen L, Winberg JO. Regulation of matrix metalloproteinase activity in health and disease. Febs J. 2011;278(1):28-45.
10. Fanjul-Fernandez M, Folgueras AR, Cabrera S, Lopez-Otin C. Matrix metalloproteinases: evolution, gene regulation and functional analysis in mouse models. Biochim Biophys Acta. 2010;1803(1):3-19.
11. Troeberg L, Nagase H. Proteases involved in cartilage matrix degradation in osteoarthritis. Biochim Biophys Acta. 2012;1824(1):133-45.
12. Gompels LL, Lim NH, Vincent T, Paleolog EM. In vivo optical imaging in arthritis--an enlightening future? Rheumatology (Oxford). 2010;49(8):1436-46.
13. Edgington LE, Verdoes M, Bogyo M. Functional imaging of proteases: recent advances in the design and application of substrate-based and activity-based probes. Curr Opin Chem Biol. 2011;15(6):798-805.
14. Blum G, Mullins SR, Keren K, Fonovic M, Jedeszko C, Rice MJ, et al. Dynamic imaging of protease activity with fluorescently quenched activity-based probes. Nat Chem Biol. 2005;1(4):203-9.
15. Blum G, von Degenfeld G, Merchant MJ, Blau HM, Bogyo M. Noninvasive optical imaging of cysteine protease activity using fluorescently quenched activity-based probes. Nat Chem Biol. 2007;3(10):668-77.
16. Edgington LE, Berger AB, Blum G, Albrow VE, Paulick MG, Lineberry N, et al. Noninvasive optical imaging of apoptosis by caspase-targeted activity-based probes. Nat Med. 2009;15(8):967-73.
17. Weissleder R, Tung CH, Mahmood U, Bogdanov A, Jr. In vivo imaging of tumors with protease-activated near-infrared fluorescent probes. Nat Biotechnol. 1999;17(4):375-8.
18. Jaffer FA, Kim DE, Quinti L, Tung CH, Aikawa E, Pande AN, et al. Optical visualization of cathepsin K activity in atherosclerosis with a novel, protease-activatable fluorescence sensor. Circulation. 2007;115(17):2292-8.

19. Caglic D, Globisch A, Kindermann M, Lim NH, Jeske V, Juretschke HP, et al. Functional in vivo imaging of cysteine cathepsin activity in murine model of inflammation. Bioorg Med Chem. 2011;19(3):1055-61.
20. Li J, Chen K, Liu H, Cheng K, Yang M, Zhang J, et al. Activatable near-infrared fluorescent probe for in vivo imaging of fibroblast activation protein-alpha. Bioconjug Chem. 2012;23(8):1704-11.
21. Chen J, Tung CH, Allport JR, Chen S, Weissleder R, Huang PL. Near-infrared fluorescent imaging of matrix metalloproteinase activity after myocardial infarction. Circulation. 2005;111(14):1800-5.
22. Jiang T, Olson ES, Nguyen QT, Roy M, Jennings PA, Tsien RY. Tumor imaging by means of proteolytic activation of cell-penetrating peptides. Proc Natl Acad Sci U S A. 2004;101(51):17867-72.
23. Watzke A, Kosec G, Kindermann M, Jeske V, Nestler HP, Turk V, et al. Selective activity-based probes for cysteine cathepsins. Angew Chem. 2008;47(2):406-9.
24. Buchardt J, Schiodt CB, Krog-Jensen C, Delaisse JM, Foged NT, Meldal M. Solid phase combinatorial library of phosphinic peptides for discovery of matrix metalloproteinase inhibitors. J Comb Chem. 2000;2(6):624-38.
25. Meldal M, Holm CB, Bojesen G, Jakobsen MH, Holm A. Multiple column peptide synthesis, Part 2 (1, 2). Int J Pept Protein Res. 1993;41(3):250-60.
26. Troeberg L, Tanaka M, Wait R, Shi YE, Brew K, Nagase H. E. coli expression of TIMP-4 and comparative kinetic studies with TIMP-1 and TIMP-2: insights into the interactions of TIMPs and matrix metalloproteinase 2 (gelatinase A). Biochemistry. 2002;41(50):15025-35.
27. Devel L, Rogakos V, David A, Makaritis A, Beau F, Cuniasse P, et al. Development of selective inhibitors and substrate of matrix metalloproteinase-12. J Biol Chem. 2006;281(16):11152-60.
28. Yu Z, Visse R, Inouye M, Nagase H, Brodsky B. Defining the requirements for collagenase cleavage in collagen type III using a bacterial collagen system. J Biol Chem. 2012.
29. Nuti E, Casalini F, Avramova SI, Santamaria S, Cercignani G, Marinelli L, et al. N-O-isopropyl sulfonamido-based hydroxamates: design, synthesis and biological evaluation of selective matrix metalloproteinase-13 inhibitors as potential therapeutic agents for osteoarthritis. J Med Chem. 2009;52(15):4757-73.
30. Inglis JJ, Simelyte E, McCann FE, Criado G, Williams RO. Protocol for the induction of arthritis in C57BL/6 mice. Nat Protoc. 2008;3(4):612-8.
31. Matsumoto S, Kobayashi T, Katoh M, Saito S, Ikeda Y, Kobori M, et al. Expression and localization of matrix metalloproteinase-12 in the aorta of cholesterol-fed rabbits: relationship to lesion development. Am J Pathol. 1998;153(1):109-19.
32. Ryu JH, Lee A, Chu JU, Koo H, Ko CY, Kim HS, et al. Early diagnosis of arthritis in mice with collagen-induced arthritis, using a fluorogenic matrix metalloproteinase 3-specific polymeric probe. Arthritis Rheum. 2011;63(12):3824-32.
33. Dean RA, Cox JH, Bellac CL, Doucet A, Starr AE, Overall CM. Macrophage-specific metalloelastase (MMP-12) truncates and inactivates ELR+ CXC chemokines and generates CCL2, -7, -8, and -13 antagonists: potential role of the macrophage in terminating polymorphonuclear leukocyte influx. Blood. 2008;112(8):3455-64.
34. Gent YY, Voskuyl AE, Kloet RW, van Schaardenburg D, Hoekstra OS, Dijkmans BA, et al. Macrophage PET imaging as biomarker for preclinical rheumatoid arthritis. Arthritis Rheum. 2011.
35. Verstappen SM, Poole AR, Ionescu M, King LE, Abrahamowicz M, Hofman DM, et al. Radiographic joint damage in rheumatoid arthritis is associated with differences in

cartilage turnover and can be predicted by serum biomarkers: an evaluation from 1 to 4 years after diagnosis. Arthritis Res Ther. 2006;8(1):R31.
36. Neuhold LA, Killar L, Zhao W, Sung ML, Warner L, Kulik J, et al. Postnatal expression in hyaline cartilage of constitutively active human collagenase-3 (MMP-13) induces osteoarthritis in mice. J Clin Invest. 2001;107(1):35-44.
37. Booth G, Newham P, Barlow R, Raines S, Zheng B, Han S. Gene expression profiles at different stages of collagen-induced arthritis. Autoimmunity. 2008;41(7):512-21.
38. Lee S, Park K, Lee SY, Ryu JH, Park JW, Ahn HJ, et al. Dark quenched matrix metalloproteinase fluorogenic probe for imaging osteoarthritis development in vivo. Bioconjug Chem. 2008;19(9):1743-7.
39. Visse R, Nagase H. Matrix metalloproteinases and tissue inhibitors of metalloproteinases: structure, function, and biochemistry. Circ Res. 2003;92(8):827-39.
40. Fingleton B. MMPs as therapeutic targets--still a viable option? Semin Cell Dev Biol. 2008;19(1):61-8.

Tables:

Table 1: Rates of cleavage of substrates by different MMPs (nmols sec^{-1}) in 50 mM Tris-HCl pH 7.5, 150 mM NaCl, 10 mM $CaCl_2$, 0.05% Brij-35 at 37 ^oC.

Substrate	MMP-1_{cat}	MMP-2	MMP-3_{cat}	MMP-12	MMP-13
MMP12-1	0.025	0.015	0.015	1.066	0.089
MMP12-2	0.013	0.011	0.011	0.339	0.012
MMP13-1	0.008	0.002	0.005	0.006	0.006
MMP13-2	0.032	0.026	0.020	0.186	0.428

Table 2: Pearson correlation (*r*) of CIA severity (paw thickness) with *MMP12ap* and *MMP13ap* activation.

Days after onset		3	5	10	15	3 + 5	All
MMP12ap	n	4	11	6	4	15	25
	r	0.991	0.759	-0.031	0.488	0.847	0.416
	p	0.009	0.007	0.953	0.512	<0.0001	0.039
MMP13ap	n	14	7	12	16	21	48
	r	0.423	0.833	0.362	0.462	0.518	0.581
	p	0.132	0.02	0.247	0.072	0.016	<0.0001

Figure Legends:

Figure 1: Chemical structures and specificity of *MMP12ap* and *MMP13ap*

A The structures of *MMP12ap* (QSY-GPLG~LEEAK(Cy5.5)G) and *MMP13ap* (QSY21-GGPAG~LYEK(Cy5.5)G) (~ denotes the cleavage site). **B** Fluorescence images of 5 µl solutions of 1 µM *MMP12ap* or *MMP13ap* spotted on glass slides after incubation with 50 nM MMP-1_{cat}, MMP-2, MMP-3_{cat}, MMP-12_{cat} and MMP-13 for 30 mins at 37 ^{o}C.

Figure 2: Specific activation of *MMP12ap* and *MMP13ap* in zymosan-induced oedemas.

The inflamed right hind paws of mice were imaged at the time points indicated after intraplantar injection of the probe. *MMP12ap* is shown on the left and *MMP13ap* on the right. **A** Representative fluorescence images showing activation of the probe over time in a single animal after intraplantar injection of probe and inhibition by GM6001. **B** Graphical quantification of probe activation after intraplantar injection with or without inhibitors (n = 3). Probe alone (●), probe with GM6001 (▲), probe with MMP-12i (■) and probe with MMP-13i (○). **C** Representative Fluorescence images showing the activation of probe over time from a single animal after intravenous injection of probe. **D** Graphical quantification of activated probe after intravenous injection (n = 5). Inflamed right hind paw (●) and contralateral paw (▲) * $p < 0.05$. All data are ± s.e.m..

Figure 3: The CIA model and representative *MMP12ap* and *MMP13ap* activation images.

Ten week old DBA/1 mice were immunized with 200 µg bovine type II collagen in Freund's complete adjuvant and development of arthritis followed daily. **A** Incidence of arthritis, and

B the summed scores from all paws (maximum 12) and thickness of hind paws after onset of arthritis. All data are mean ± s.e.m.. **C** and **D** Representative images obtained 4 hours after intravenous injection of *MMP12ap* (C) and *MMP13ap* (D) with the clinical scores of the individual paws indicated.

Figure 4: Activation of the *MMP12ap* and *MMP13ap* in CIA

Mice were imaged 4 hours after intravenous injection of 150 µl 1 µM probe in the early phase (3 and 5 days) and the later phase (10 and 15 days) of disease. **A** and **B** The MFI was plotted against the hind paw thickness for 3 (○), 5 (▲), 10 (■) and 15 (Δ) days after onset of arthritis for *MMP12ap* (A) and *MMP13ap* (B) to determine the correlation between probe activation and severity of disease. The Pearson correlation coefficients are indicated for days 3-5 for *MMP12ap* and days 3-15 for *MMP13ap* with details for the individual groups in table 2. **C** and **D** Longitudinal change in *MMP12ap* (C) and *MMP13ap* (D) activation in the progression of CIA. Data are mean ± s.e.m.. See table 2 for n numbers. * $p < 0.05$ after one way ANOVA with Bonferroni post-test.

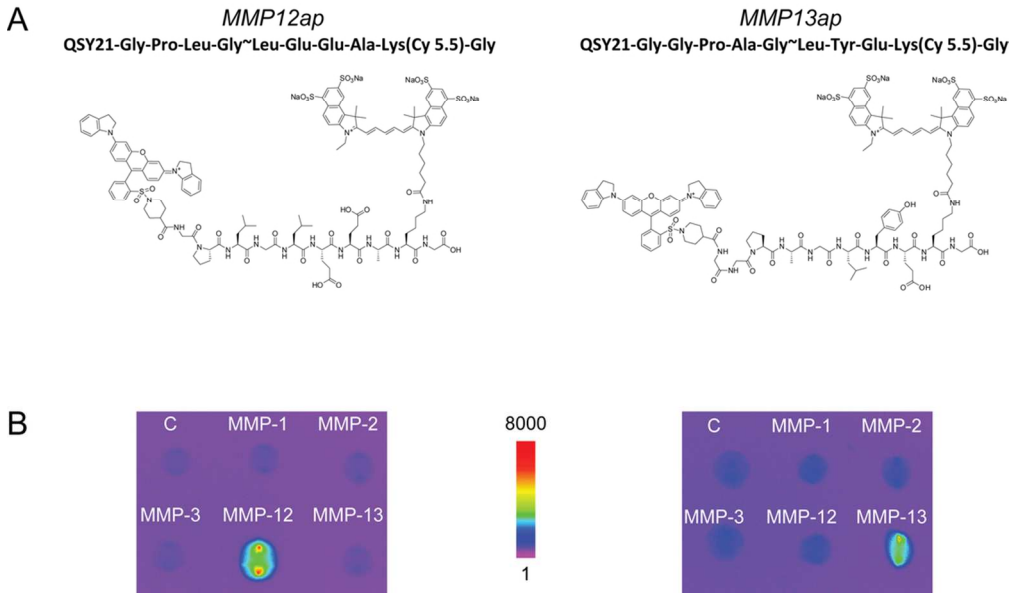

Figure 1: Chemical structures and specificity of *MMP12ap* and *MMP13ap*
A The structures of *MMP12ap* (QSY-GPLG~LEEAK(Cy5.5)G) and *MMP13ap* (QSY21-GGPAG~LYEK(Cy5.5)G) (~ denotes the cleavage site). **B** Fluorescence images of 5 µl solutions of 1 µM *MMP12ap* or *MMP13ap* spotted on glass slides after incubation with 50 nM MMP-1cat, MMP-2, MMP-3cat, MMP-12cat and MMP-13 for 30 mins at 37 °C.

101x59mm (300 x 300 DPI)

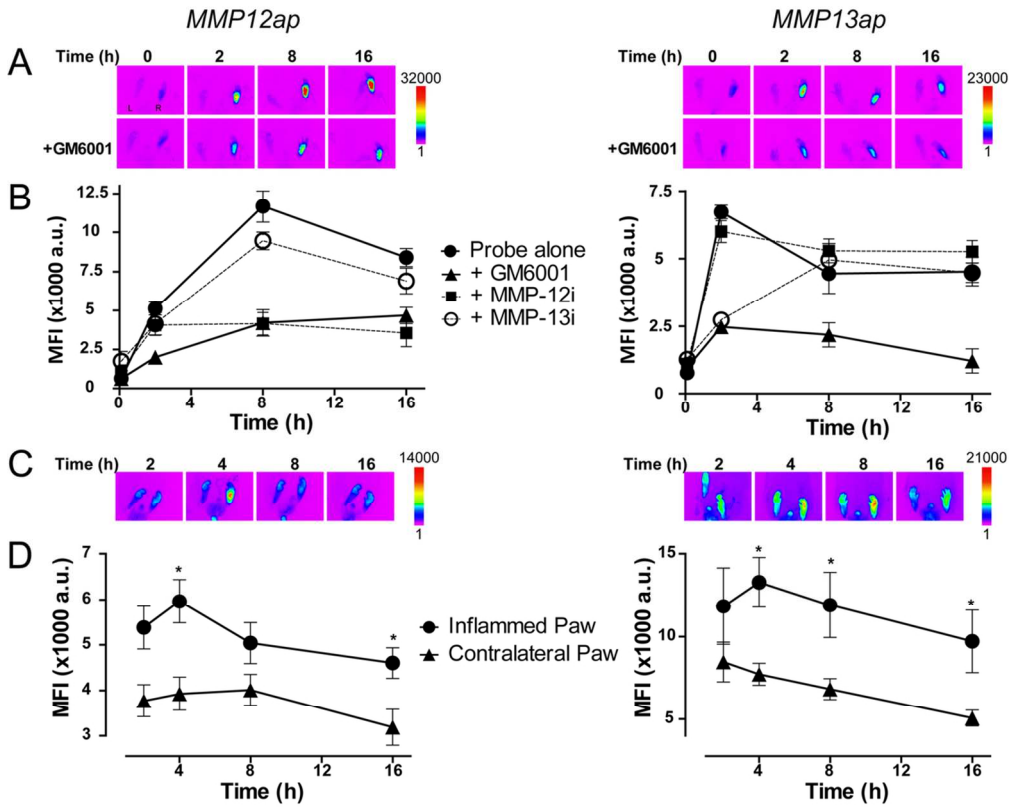

Figure 2: Specific activation of *MMP12ap* and *MMP13ap* in zymosan-induced oedemas. The inflamed right hind paws of mice were imaged at the time points indicated after intraplantar injection of the probe. *MMP12ap* is shown on the left and *MMP13ap* on the right. **A** Representative fluorescence images showing activation of the probe over time in a single animal after intraplantar injection of probe and inhibition by GM6001. **B** Graphical quantification of probe activation after intraplantar injection with or without inhibitors (n = 3). Probe alone (●), probe with GM6001 (▲), probe with MMP-12i (■) and probe with MMP-13i (○). **C** Representative fluorescence images showing the activation of probe over time from a single animal after intravenous injection of probe. **D** Graphical quantification of activated probe after intravenous injection (n = 5). Inflamed right hind paw (●) and contralateral paw (▲) * p <0.05. All data are ± s.e.m..

107x87mm (300 x 300 DPI)

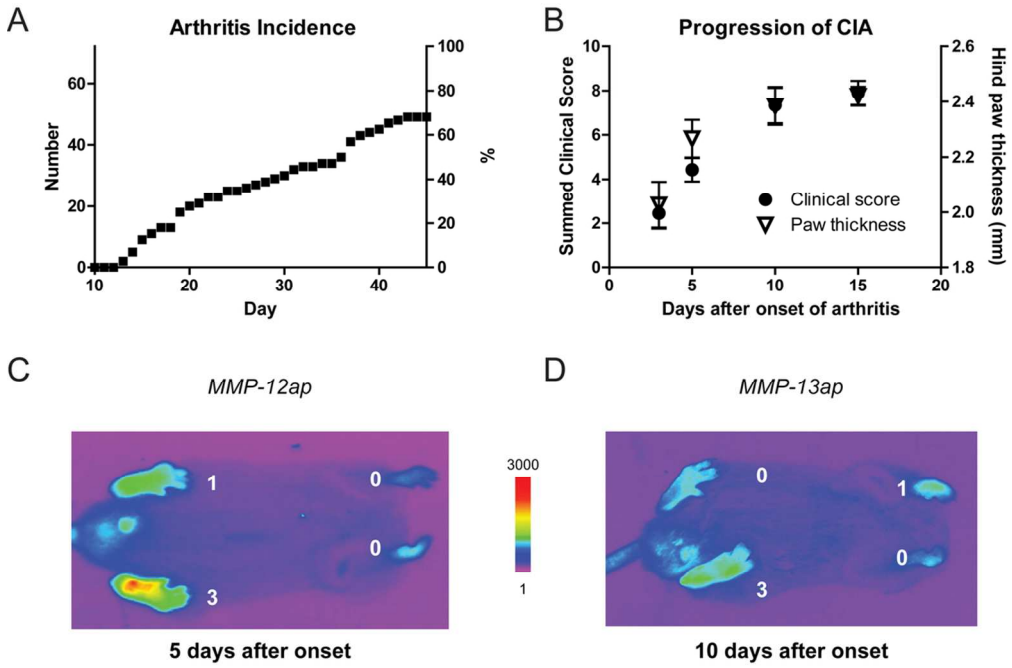

Figure 3: The CIA model and representative *MMP12ap* and *MMP13ap* activation images. Ten week old DBA/1 mice were immunized with 200 µg bovine type II collagen in Freund's complete adjuvant and development of arthritis followed daily. **A** Incidence of arthritis, and **B** the summed scores from all paws (maximum 12) and thickness of hind paws after onset of arthritis. All data are mean ± s.e.m.. **C** and **D** Representative images obtained 4 hours after intravenous injection of *MMP12ap* (C) and *MMP13ap* (D) with the clinical scores of the individual paws indicated.

107x71mm (300 x 300 DPI)

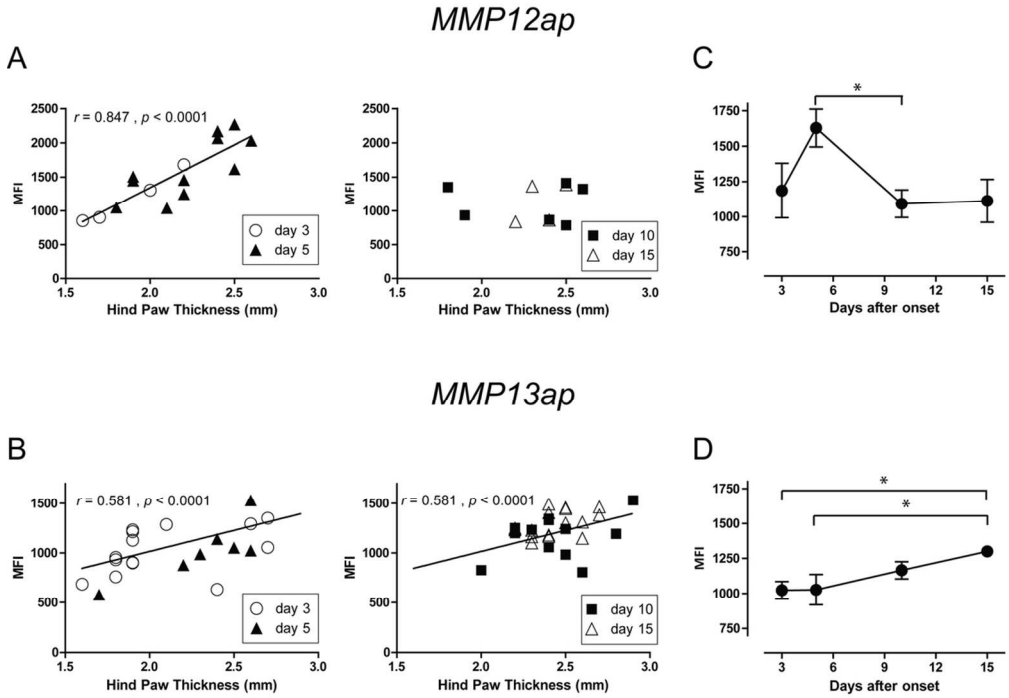

Figure 4: Activation of the *MMP12ap* and *MMP13ap* in CIA
Mice were imaged 4 hours after intravenous injection of 150 µl 1 µM probe in the early phase (3 and 5 days) and the later phase (10 and 15 days) of disease. **A** and **B** The MFI was plotted against the hind paw thickness for 3 (○), 5 (▲), 10 (■) and 15 (Δ) days after onset of arthritis for *MMP12ap* (A) and *MMP13ap* (B) to determine the correlation between probe activation and severity of disease. The Pearson correlation coefficients are indicated for days 3-5 for MMP12ap and days 3-15 for MMP13ap with details for the individual groups in table 2. **C** and **D** Longitudinal change in *MMP12ap* (C) and *MMP13ap* (D) activation in the progression of CIA. Data are mean ± s.e.m.. See table 2 for n numbers. * $p < 0.05$ after one way ANOVA with Bonferroni post-test.

107x74mm (300 x 300 DPI)